



## Altitudinal variation in impacts of snow cover, reservoirs and precipitation seasonality on monthly runoff in Tibetan Plateau catchments

Nan Wu<sup>a,b,c,f</sup>, Ke Zhang<sup>a,b,c,d,e,\*</sup>, Amir Naghibi<sup>f</sup>, Hossein Hashemi<sup>f</sup>, Zhongrui Ning<sup>b,c</sup>, Jerker Jarsjö<sup>g</sup>

<sup>a</sup>*The National Key Laboratory of Water Disaster Prevention, Hohai University, Nanjing, Jiangsu,*

5 *210024, China*

<sup>b</sup>*Yangtze Institute for Conservation and Development, Hohai University, Nanjing, Jiangsu, 210024, China*

<sup>c</sup>*College of Hydrology and Water Resources, Hohai University, Nanjing, Jiangsu, 210024, China*

<sup>d</sup>*China Meteorological Administration Hydro-Meteorology Key Laboratory, Hohai University, Nanjing,*

10 *Jiangsu, 210024, China*

<sup>e</sup>*Key Laboratory of Water Big Data Technology of Ministry of Water Resources, Hohai University, Nanjing, Jiangsu, 210024, China*

<sup>f</sup>*Division of Water Resources Engineering, LTH, Lund University, Lund, 22100, Sweden*

<sup>g</sup>*Department of Physical Geography, Stockholm University, Stockholm, 10691, Sweden;*

15 \* Corresponding author at: The National Key Laboratory of Water Disaster Prevention, Hohai University, Nanjing, Jiangsu, 210098, China

E-mail address: kzhang@hhu.edu.cn (Ke Zhang)



## ABSTRACT

Although of great importance for long-term, effective water resource allocation, current  
20 knowledge of monthly runoff variability, its spatio-temporal characteristics, and underlying  
key drivers, including their sensitivity to climate change and other human impacts, is limited.  
With a particular focus on 10 sub-basins along an elevation gradient (1000 to 5900 m.a.s.l.) in  
the hydrologically complex, seasonally cold Yalong River basin, China, this study developed  
an extended Budyko framework based on monthly water balances (2002-2016) to consider  
25 snow storage dynamics ( $\Delta S_{\text{snow}}$ ) separately from other terrestrial water storage changes ( $\Delta S$ ),  
including those related to hydropower reservoir construction. Results showed that snow  
accumulation and snowmelt are main drivers of runoff seasonality in the upper sub-catchments  
of the Yalong River basin, with propagating impacts also on lower-elevation snow-free sub-  
catchments, which are increasingly under the additional influence of hydropower reservoirs.  
30 This creates a relatively strong altitudinal heterogeneity in drivers of monthly runoff, which  
has been hypothesized to occur also in other world regions including e.g. major European rivers  
of Alpine origin, although not yet quantified at similarly high spatio-temporal resolution.  
Furthermore, an observed decrease in runoff seasonality in the Yalong River at its Yangtze  
River outlet (that receives water from all 10 investigated sub-basins) was shown to be unrelated  
35 to snow storage changes and hence likely caused by trends in unfrozen precipitation seasonality  
and/or flow-modulating impacts of constructed reservoirs, natural lakes and groundwater,  
implying that further snow thinning may exacerbate such trends in the future. Implementing  
the variance decomposition method based on the extended Budyko framework, the intra-annual



runoff variability ( $\sigma^2_R$ ) was captured by calculating the variance and covariance of influencing  
40 factors ( $R^2$  values above 0.9 in most sub-basins) with the main contributors being variances of  
rainfall ( $P_r$ ) and  $\Delta S'$ . Methodologically, we have verified the substantial contribution of  
hydropower reservoir storage changes on total storage changes by independent analysis of  
reservoir storage data, supporting the applicability of the extended monthly Budyko framework  
for identifying dominant processes in the context of runoff generation and the rapid  
45 environmental changes that the Yalong River basin and other cold regions (not least of the  
Tibetan plateau) are currently experiencing.

**Keywords:** Runoff variability, Snowmelt, Terrestrial storage change, Altitudinal trend,  
Correlation analysis, Budyko framework, Yalong River basin

## 1. Introduction

50 Runoff is a key component of the hydrological cycle and is highly susceptible to external  
environmental factors, primarily climate change and human activities, which can lead to  
significant changes in hydrological processes (Bao et al., 2023). Climate variations such as  
precipitation intensity, rising temperature, and enhanced radiation not only affect the water  
vapor content in the atmosphere but also alter the surface characteristics of catchments (Li and  
55 Quiring, 2021). Moreover, extensive human activities such as reservoir construction increase  
the complexity of surface water flow, making accurate analysis of the hydrological cycle a  
challenge (Gutenson et al., 2020). Observations indicate that 24% of the global river flow has  
undergone significant changes (Li et al., 2020). Runoff changes, influenced by evolving factors  
(Yao et al., 2020), show the sensitivity of hydrological cycles to climate conditions and surface



60 characteristics (Huang et al., 2021). While intra-annual analysis of runoff response to climate variability and change provides vital information for the effective allocation of water resources, a significant amount of research is focused on multi-annual timescale analysis (Huo et al., 2021; Ning et al., 2017; Tu et al., 2015). Changes in monthly climate conditions and human activities largely drive variations in monthly runoff (Xin et al., 2019; Yao et al., 2020).

65 In many parts of the world, seasonal storage of snow and ice provides meltwater and secures water supply over the growing season. Although climate change impacts frequently act to reduce seasonal volumes of stored snow and ice, it is challenging to predict the consequences for runoff. This is partly due to the difficulty of disentangling such impacts from other influences on runoff, such as changes in precipitation and temperature, and reservoir  
70 construction. Benchmark estimates have shown that that snowmelt during the rainy season (April to June) contributed to 31% of the annual runoff for the source regions of the Indus River, while the source regions of the Yellow River, Yangtze River, Mekong River, Thanlwin River, and Brahmaputra River received snowmelt from April to June, contributing to 20-23% of the annual runoff (Zhang et al., 2013). Additionally, the snowfall-to-precipitation ratio has been  
75 found to exert a significant influence on both annual runoff and intra-annual runoff variation (Berghuijs et al., 2014; Liu et al., 2022; Zhang et al., 2015).

Recent studies on this topic have also shown evidence of decreased runoff seasonality, e.g. in snow-dominated rivers of central Europe (Rottler et al., 2020). In cold regions of China, water storage and runoff characteristics show quite complex spatio-temporal patterns over the  
80 last 30 years (Fang et al., 2019). This is particularly the case in the downstream regions that use reservoirs to alter the intra-annual hydrological cycle and store water to ensure a sustainable





water supply during dry seasons in the face of agricultural, industrial, and domestic demands  
(Shen, 2018). More generally, water storage in lakes, reservoirs and groundwater aquifers  
may contribute considerably to monthly runoff dynamics (Bai et al., 2018; Hwang and  
85 Devineni, 2022; Shi and Gao, 2022). It is hence most likely that distinct differences in drivers  
of monthly runoff exist across altitudinal gradients of different mountainous regions of the  
world (Kuhn et al., 2016; Rottler et al., 2020; Shen, 2018), although the details of such patterns  
are largely unexplored. Zhang et al. (Zhang et al., 2016) emphasized that main factors (e.g.,  
human activities and climate-driven changes in runoff) that affect the runoff variance deserve  
90 more attention. A more detailed understanding intra-annual runoff characteristics in  
mountainous watersheds under changing environments combined with attribution analyses are  
crucial for sustainable water resource management (Dethier et al., 2020; Liu et al., 2017).

Precipitation and potential evapotranspiration define catchment water availability and  
storage capacity (Huang et al., 2021; Li et al., 2021; Yao et al., 2020). On a multi-year scale,  
95 precipitation is partitioned into evapotranspiration and runoff, reflecting competition between  
water supply (precipitation) and available energy (potential evapotranspiration) and regulated  
by the corresponding underlying surface characteristics (Wu et al., 2018). To analyze annual  
and multi-year scale hydrological processes considering rainfall and runoff changes, the  
Budyko framework has been widely used (Choudhury, 1999) The framework was initially  
100 developed to address water resource constraints through multi-year averages (Kazemi et al.,  
2021; Wang and Tang, 2014; Yang et al., 2008; Zhang et al., 2004) and has been widely applied  
to quantitatively analyze the impact of climate change and human activity on runoff (Liu et al.,  
2021; Wang and Tang, 2014; Xu et al., 2014). However, since this framework assumes multi-



year, steady-state conditions, it is not applicable at intra-annual timescales. Furthermore, most  
105 assessments investigate the main drivers only by comparing runoff sensitivity, rather than their  
relative contribution to the actual variance of runoff (Liu et al., 2019).

Recently, some studies have attempted to extend the Budyko framework to intra-annual  
timescales, mainly by including monthly terrestrial water storage changes as part of the water  
supply (Du et al., 2016; Liu et al., 2019) and establishing a new water supply-demand  
110 relationship on monthly scale (Huang et al., 2021; Wu et al., 2019). Other studies have also  
integrated monthly terrestrial water storage in water balance using the Budyko framework  
along with hydrological models (Yao et al., 2020; Zhang et al., 2020). Some studies have  
demonstrated that incorporating terrestrial water storage significantly enhances predictability  
compared to the previous precipitation and potential evapotranspiration relationship (Wu et al.,  
115 2018; Zhang et al., 2010). Although the extended Budyko framework has been effective to  
analyze monthly runoff changes, the attribution analysis of intra-annual runoff changes needs  
to consider more driving factors, particularly due to the complexity and interaction of climate  
change and human activities in the cold mountainous regions (Liu et al., 2018; Luo and Lau,  
2018). Equally important from a process understanding perspective is the consideration of  
120 sufficiently fine-resolved temporal and spatial scales (Fang et al., 2016).

The Qinghai-Tibet Plateau, often referred to as the "Third Pole," is a region where the  
atmosphere, hydrosphere, cryosphere, and biosphere intricately interact (Bao et al., 2023; Cui  
et al., 2023). Snow accumulation begins in the fall, lasting until the subsequent spring, and in  
some high-altitude areas, snow cover persists even into the summer months (Wang et al., 2018;  
125 Wu et al., 2012). Snowmelt runoff stands as a crucial component of the primary runoff source



on the Qinghai-Tibet Plateau, exhibiting distinct seasonal variations and primarily impacting spring runoff (Gao et al., 2017; Han et al., 2019).

We here consider the Yalong River basin, situated between 1000 and 5900 m.a.s.l. in the southeastern part of the Tibetan Plateau, which experiences seasonal snow cover in its upstream regions, while the construction of downstream cascade hydropower stations has greatly affected terrestrial water storage capacity. These factors exert significant influences on regional water cycling, especially at the intra-annual scales (Wang et al., 2018; Wu and Shen, 2007). Therefore, this study aims to (1) extend the Budyko framework to distinguish between snow storage change ( $\Delta S_{snow}$ ) and remaining water storage change ( $\Delta S'$ ) in monthly water balances; (2) determine interannual and intra-annual variations of hydrological variables including runoff ( $R$ ), rainfall ( $P_r$ ), snowmelt ( $S_{melt}$ ), evapotranspiration ( $E$ ) and terrestrial water storage change ( $\Delta S$ ) in nested catchments along a pronounced altitudinal gradient, and (3) examine how relationships between runoff and other factors can vary with elevation, including assessments of major contributors to runoff variation (using variance decomposition analysis); and (4) discuss wider implications including the susceptibility of the identified monthly runoff contributors to climate-change and other human impacts.

## 2. Methods and application

In this section, the theoretical framework for attributing runoff variability based on the extended Budyko is described in Sect. 2.1. Then, the implementation of the extended Budyko framework is explained in Sect. 2.2. Table 1 presents the variables and acronyms used in this study.



**Table 1.** Description of hydrological variables and acronyms.

| Number | Variable (mm)  | Abbreviation                             |
|--------|--|--|
| 1      | Precipitation  | $P$                                      |
| 2      | Rainfall component of $P$                            | $P_r$                                    |
| 3      | Snowfall component of $P$                            | $P_s$                                    |
| 4      | Total available water                                | $P'$                                     |
| 5      | Potential evapotranspiration                         | $E_0$                                    |
| 6      | Actual evapotranspiration                            | $E$                                      |
| 7      | Runoff   | $R$                                      |
| 8      | Change in terrestrial water storage                  | $\Delta S$                               |
| 9      | Change in ground snowpack storage                    | $\Delta S_{snow}$                        |
| 10     | Differences between $\Delta S$ and $\Delta S_{snow}$ | $\Delta S' = \Delta S - \Delta S_{snow}$ |
| 11     | Snow melt  | $S_{melt}$                               |

## 2.1. Methods

Figure 1 provides an overview of the extended Budyko calculation for the present study.

150 Observation data on temperature  $T$ , precipitation  $P$  and runoff  $R$  were used to resolve monthly water balances, and for estimation of multiple hydrological variables (included in Table 1) in ten sub-basins of the Yalong River basin. In addition to two relatively large headwater catchments and four smaller ones, we here consider four nested catchment areas (see further the study area description of Sect. 2.2.1) for which the net runoff  $R$  at any particular time is

155 quantified as the difference in measured discharges  $\Delta Q = Q_{down} - Q_{up}$  between the downstream discharge station and upstream discharge station, divided by the corresponding difference in catchment areas  $\Delta A = A_{down} - A_{up}$ . For the headwater catchments,  $Q_{up}$  and  $A_{up}$  are per definition equal to zero. The water balance variables were then used as input to an extended Budyko framework. Subsequently, the correlation between monthly  $R$  and the hydrological variables

160 (including drivers of  $R$ , such as  $P_r$ ,  $S_{melt}$ ,  $\Delta S$ , and  $E$ ; Table 1) was explored, focusing on the lag time of  $R$  response to  $P$  events. Finally, the relative contributions of driving factors to monthly



runoff variability were quantitatively assessed using the variance decomposition method. The hydrological variables employed in this study are shown in Table 1.

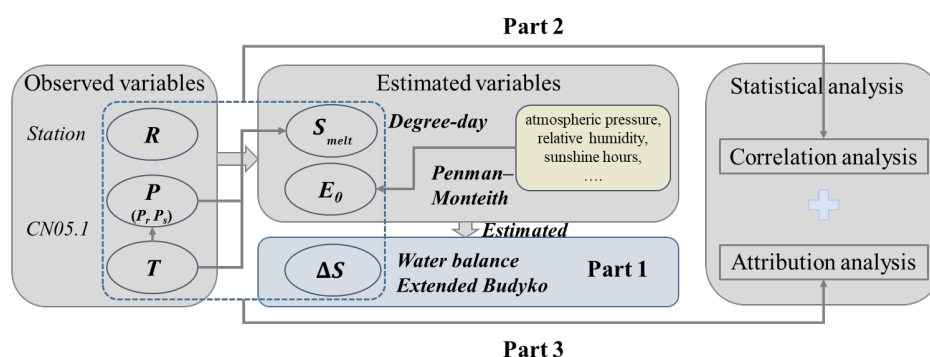


**Figure 1.** Flowchart of the extended Budyko framework. Italic text represents the data source, and italic-  
 bold text represents the calculation method for obtaining the data.

### 2.1.1 Extended Budyko framework by decomposing $\Delta S$

The present analyses use water balance methods based on the Budyko hydrothermal coupling theory, which compared with statistical empirical methods possesses substantial physical significance and is straightforward to calculate and parameterize (Hwang and Devineni, 2022; Shi and Gao, 2022). The partitioning of annual precipitation into annual evapotranspiration and streamflow is determined by the competition between available water and available energy measured by potential evapotranspiration (Huang et al., 2021), and many scholars have proposed empirical equations to characterize this relationship that is a part of the Budyko framework (Choudhury, 1999; Wang and Tang, 2014; Yang et al., 2008; Zhang et al., 2004). However, due to their simplicity and effectiveness, some of those equations have been applied more than others. We consider one of the most popular equations, namely Choudhury-Yang:



$$E = \frac{P \times E_0}{(P^n + E_0^n)^{1/n}} \quad (1)$$

where potential evapotranspiration ( $E_0$ , mm) and precipitation ( $P$ , mm) act as indicators  
 180 for energy and water supply, respectively, and where  $E$  (mm) is the calculated actual  
 evapotranspiration, and  $n$  is a landscape parameter, mainly expressing impacts of prevailing  
 surface conditions within the basin.

The water balance equation on the decadal time scale for a basin can be expressed using  
 equation (2), wherein  $P$  represents the total water input to the basin. The outputs comprise  
 185 runoff ( $R$ , mm) and evapotranspiration ( $E$ , mm).

$$P = R + E \quad (2)$$

The change in terrestrial water storage can be assumed to be approximately 0 on the  
 decadal time scale, while on the intra-annual time scale, it cannot be neglected (Huang et al.,  
 2021; Xu et al., 2012):

$$P = R + E + \Delta S \quad (3)$$

In order to consider the dynamic changes of monthly snow accumulation and melting  
 190 separately,  $P$  was differentiated into rainfall ( $P_r$ , mm) and snowfall ( $P_s$ , mm) using daily  
 temperature thresholds (Widen-Nilsson et al., 2007), and the terrestrial water storage change  
 was also divided into two components: one accounts for snow storage change ( $\Delta S_{snow}$ , mm),  
 and the other represents the remaining storage changes ( $\Delta S'$  mm; mainly including storage  
 changes in surface water, groundwater and soil water). Thus, Equation (3) can be expressed as:

$$P_r + P_s = R + E + \Delta S_{snow} + \Delta S' \quad (4)$$

195 In this study, the cumulative value of daily  $P_r$  (and  $P_s$ ) was calculated based on daily  
 temperature to derive monthly  $P_r$  (and  $P_s$ ).  $\Delta S_{snow}$  is mainly supplied in solid form by  $P_s$  and



depleted in liquid form by melting snow ( $S_{melt}$ , mm). Equation (4) can then be expressed as:

$$P_r + P_s = R + E + (P_s - S_{melt}) + \Delta S' \quad (5)$$

The monthly water balance equation can be written as:

$$P_r + S_{melt} = R + E + \Delta S' \quad (6)$$

Therefore, the total available water ( $P'$ ) for  $E$  and  $R$  is expressed as the sum of  $P_r$ ,  $S_{melt}$

200 and  $\Delta S'$  (Zeng and Cai, 2015). Accordingly, Equation (6) can be modified as follows:

$$P' = P_r + S_{melt} - \Delta S' = R + E \quad (7)$$

Combining equation (1) and equation (7), an extended Budyko framework with a parameter  $n$  can be formulated as:

$$E = \frac{(P_r + S_{melt} - \Delta S') \times E_0}{((P_r + S_{melt} - \Delta S')^n + E_0^n)^{1/n}} \quad (8)$$

In this study, the Penman-Monteith method (Allen et al., 1998) was used for  $E_0$  calculation, e.g. in consistency with the FAO Irrigation and Drainage Paper No. 56 (Allen et al., 1998) showing that the Penman-Monteith model is a preferable physical approach to estimate  $E_0$ . It is often utilized as a standard method for verifying other empirical methods (Chen et al., 2005). The Penman-Monteith method has also been widely employed for estimating evapotranspiration on snow surfaces (Stigter et al., 2018; Xin et al., 2021), considering it a saturated or unstressed surface similar to water surfaces (Yang and Bai, 2023). Due to the high albedo of snow surface, the surface radiance is typically higher than that of the air, resulting in negative net radiation for many snow-covered pixels. Currently, the evaporation mechanism under negative net radiation conditions is under-studied. Therefore, in this study,  $E$  is assumed to be 0 when the net radiation is less than 0 (Gan et al., 2022).

210

Therefore, the monthly runoff  $R$  can be expressed as:



$$R = P_r + S_{melt} - \Delta S' - \frac{(P_r + S_{melt} - \Delta S') \times E_0}{((P_r + S_{melt} - \Delta S')^n + E_0^n)^{1/n}} \quad (9)$$

215 in which  $R$  was obtained from direct discharge measurements, and  $S_{melt}$  was computed using the degree-day method. The  $n$  parameter is primarily employed to characterize the underlying surface conditions of the basin, including factors such as average slope (Zhang et al., 2004) and vegetation type or land use (Bounoua et al., 2004), which might undergo significant changes on long-term scales, whereas differences over short-term scales, such as 220 monthly, are typically minimal. Therefore, based on a previous study (Huang et al. 2021) we assumed that  $n$  can be treated as constant value for monthly and multi-year scales. We hypothesized and tested our assumption,  $n$ , by calculating the evapotranspiration using the Budyko and extended Budyko. As shown in Table S1, the results showed a high correlation coefficient between the evapotranspiration values in both models, which supports our 225 hypothesis. Thus, the monthly  $\Delta S'$  was calculated by closing the water balance.

The degree-day method relies on readily available data and straightforward calculations, providing comparable accuracy to the energy balance method at the basin scale (Hock, 2003). The degree-day model operates on the assumption of a strong positive linear correlation between temperature and  $S_{melt}$ , with the fundamental equation depicted in equation (10). If the 230 daily temperature  $T_i$  surpasses the temperature threshold  $T_0$ , the  $S_{melt}$  is determined by the degree-day factor ( $D$ , mm/°C/day) and temperature:

$$S_{melt} = D \times (T_i - T_0) \quad \text{if } T_i > T_0 \quad (10)$$

In this method, the parameter  $D$  typically falls within the range of 2.5-14 mm/°C/day, with specific values described in Sect. 2.2.2.  $T_0$  is commonly assumed to be 0°C, and  $S_{melt}$  is





constrained by the presence of existing snow depth.

### 2.1.2. Cross correlation analysis

Runoff is influenced by various natural and geographical factors, such as climate and the underlying surface. Precipitation serves as the primary driving factor in the formation of runoff. Following intricate surface and subsurface hydrological processes, catchment responses to precipitation gradually undergoes smoothing and lagging (Brutsaert and Hiyama, 2012) the hysteresis relationship between monthly precipitation and runoff within Yalong River basin, the variable  $\tau$  to compute the lag time between the precipitation events and subsequent runoff changes, ranging from 0 to 5 months. Statistical significance was considered as  $p \leq 0.05$  for this analysis.

### 2.1.3. Quantifying the contributions of different factors to runoff variability

Equation (9) could be expressed as  $R = f(P_r, S_{melt}, \Delta S', E_0)$ . The variance of  $R$  (within a year is determined by the variance of each driving factor ( $P_r, S_{melt}, \Delta S', E_0$ ) and their covariance (Ye et al., 2015):

$$\begin{aligned} \sigma_R^2 = & \left(\frac{\partial f}{\partial P_r}\right)^2 \sigma_{P_r}^2 + \left(\frac{\partial f}{\partial S_{melt}}\right)^2 \sigma_{S_{melt}}^2 + \left(\frac{\partial f}{\partial \Delta S'}\right)^2 \sigma_{\Delta S'}^2 + \left(\frac{\partial f}{\partial E_0}\right)^2 \sigma_{E_0}^2 + 2\left(\frac{\partial f}{\partial P_r}\right. \\ & \cdot \frac{\partial f}{\partial S_{melt}}\bigg)cov(P_r, S_{melt}) + 2\left(\frac{\partial f}{\partial P_r} \cdot \frac{\partial f}{\partial \Delta S'}\right)cov(P_r, \Delta S') + 2\left(\frac{\partial f}{\partial P_r} \right. \\ & \cdot \frac{\partial f}{\partial E_0}\bigg)cov(P_r, E_0) + 2\left(\frac{\partial f}{\partial S_{melt}} \cdot \frac{\partial f}{\partial \Delta S'}\right)cov(S_{melt}, \Delta S') + 2\left(\frac{\partial f}{\partial S_{melt}} \right. \\ & \cdot \frac{\partial f}{\partial E_0}\bigg)cov(S_{melt}, E_0) + 2\left(\frac{\partial f}{\partial \Delta S'} \cdot \frac{\partial f}{\partial E_0}\right)cov(\Delta S', E_0) \end{aligned} \quad (11)$$

Hence, equations (10) are utilized to compute the contributions of the variance of each driving factor ( $P_r, S_{melt}, \Delta S', E_0$ ) and their covariance to intra-annual runoff variability for the period 2002-2016.



## 2.2. Study area and data

### 2.2.1. Study area

The Yalong River is the largest tributary of the Jinsha River, which is made up of the upper reaches of the Yangtze River. Being a basin that encompasses a wide range of altitudes (1,000 to 5,900 m.a.s.l.) and hydro-climatic conditions (see below) while being increasingly impacted by human activities including hydropower expansion, it serves as a case study to test our method. It traverses from northwest to southeast, boasting a total length of 1,570 km and a drainage basin area of 128,000 km<sup>2</sup>. Meteorological observations in the upper reaches of the basin are limited due to the complex topography (Fig. 2). The precipitation and temperature in the Yalong River basin increases from north to south, with an average annual temperature of -3 in the north to 26 °C in the south in summer and -18 in the north to 14 °C in the south in winter. The precipitation ranges from 600 to 800 mm in the upper region, 1,000 to 1,400mm in the middle region, and 900 to 1,300 mm in the lower region. June to October is the rainy season. The annual average discharge at its confluence with the Yangtze River is 1,900 m<sup>3</sup>/s, with an annual discharge of nearly 60 billion m<sup>3</sup>, representing 13% of the total water volume upstream of the Yangtze River (He et al., 2015).

The Yalong River is renowned for its abundant hydropower resources and the middle and lower reaches are designated to the national hydropower base, ranking third among the 13 hydropower bases in China (Wu and Shen, 2007). In the downstream reaches, the construction of five hydropower stations, including Jinping I (2013), Jinping II (2013), Guandi (2012), Ertan (1999), and Tongzilin (2015), has significantly altered the terrestrial water storage (Wu and Shen, 2007). For this study, the Yalong River basin was divided into ten sub-basins based on



the distribution of hydrological stations, as depicted in Figure 2. Station coordinates and basic hydrological and meteorological data of the respective sub-basins are given in Table S2.

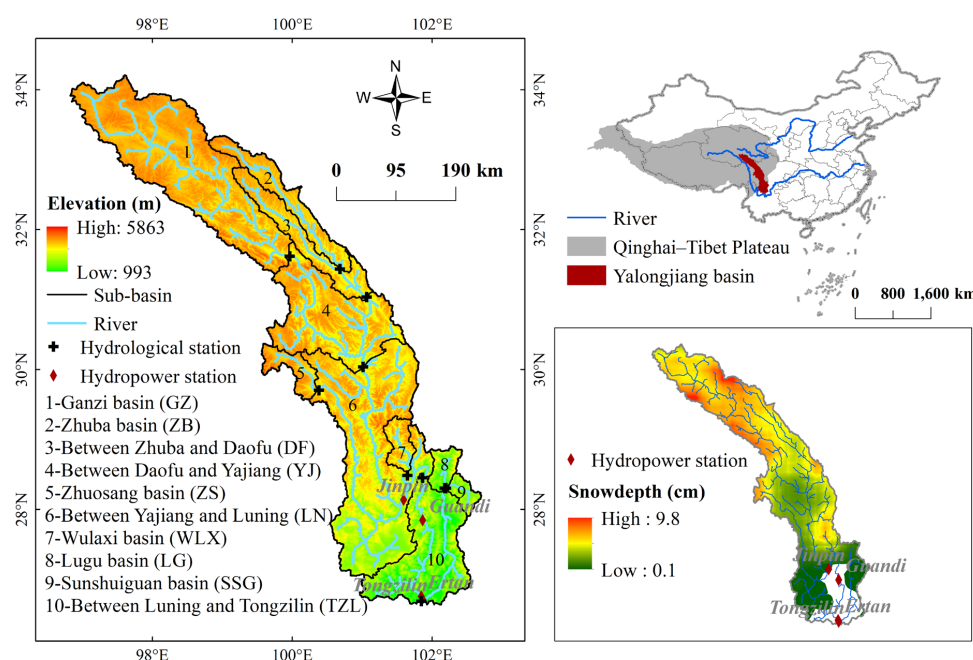


**Figure 2.** Geographic location of the sub-basins (1-10) and mean yearly average snow depth from 2002 to 2016 in the Yalong River basin.

### 2.2.2. Dataset

The average monthly runoff records during the period 2002-2016 at 10 hydrometry stations were obtained from the China Hydrological Yearbook provided by the Ministry of Water Resources of China. Table S1 gives information about the locations of stations and their corresponding sub-basins, including runoff, precipitation, temperature, and potential evapotranspiration. The first column represents the labels of the 10 sub-basins, as depicted in Figure 2, with the Tongzilin Hydrological Station serving as the controlling station for the entire Yalong River basin.



For meteorological data, the CN05.1 dataset (1961-2020) was utilized in this study, which provides a daily grid resolution of  $0.25^{\circ} \times 0.25^{\circ}$ , covering various meteorological variables, including precipitation, temperature, atmospheric pressure, relative humidity, sunshine hours, and wind speed across China. The dataset has been generated by interpolation of data from over 2,400 observation stations throughout China using the "abnormal method" (New et al., 2000). This study used a dataset of the spatial distribution of degree-day factors for glaciers and snow in High Mountain Asia, which was derived from observations over 40 glaciers. The spatial resolution of this dataset is  $0.5^{\circ}$ , with units of  $\text{mm}/^{\circ}\text{C}/\text{day}$  (Zhang et al., 2019). The evapotranspiration data was derived from GLEAM (Global Land-surface Evaporation: the Amsterdam Methodology) (1980-2020), which combines a wide range of remote sensing observations to derive daily actual evapotranspiration and its different components, including snow sublimation (Miralles et al., 2011).

### 3. Results

#### 3.1. Intra-annual changes in hydrological variables

Figure 3 depicts the full time series of  $P_r$ ,  $S_{melt}$ ,  $E$ ,  $R$ ,  $\Delta S_{snow}$ , and  $\Delta S$  of 10 sub-basins within the Yalong River basin from 2002 to 2016. It should be noted that  $R$  refers to the net runoff generated locally within the sub-basin, which in case of nested basins (DF, YJ, LN and TZL) excludes flows generated by areas further upstream. Figure 3 shows that  $P_r$  exhibited pronounced interannual variation and was additionally higher in downstream areas.  $S_{melt}$  and  $\Delta S_{snow}$  primarily occurred in the middle and upper reaches, including upstream sub-basins such as GZ, ZB, DF and YJ (Figure 3). Lower reaches subbasins with  $\Delta S_{snow} = 0$  (WLX, LG, SSG,



TZL) would hence per definition have  $\Delta S = \Delta S'$ . Within upstream areas  $E$  approached zero in the winter. Notably, the  $R$  and  $\Delta S$  in WLX underwent an abrupt change in 2009, demonstrating a significant decrease in  $R$  and general increases in  $\Delta S$ . The  $R$  decrease may in part be caused  
310 by filling of reservoirs and reservoir-induced increases in  $\Delta S$ . In LN, the  $R$  and  $\Delta S$  began to change around 2013, with locally created  $R$  fluctuating gently and  $\Delta S$  starting to show pronounced intra-annual fluctuations including considerably higher positive values, which is consistent with the construction period of the Jinping hydropower station including the filling of the dam and the start of intra-annual flow regulations. Additionally, the periodic  
315 characteristics of  $R$  (more runoff in summer and less in winter) in lower elevation regions of LG and TZL were not as clear as in other regions, and the amplitude of  $\Delta S$  varied significantly, including sharp transitions. There were even individual negative values of net  $R$  in TZL. Such phenomena are closely related to the influence of reservoirs (including hydropower dams) on the net runoff in nested catchment segments, where monthly outflow may be lower than  
320 monthly inflow, for instance when a hydropower dam near the outlet of a nested catchment temporarily stores more water ( $\Delta S_{dam}$ ) than what is created from local (positive)  $R + \Delta S$  just upstream of the dam.

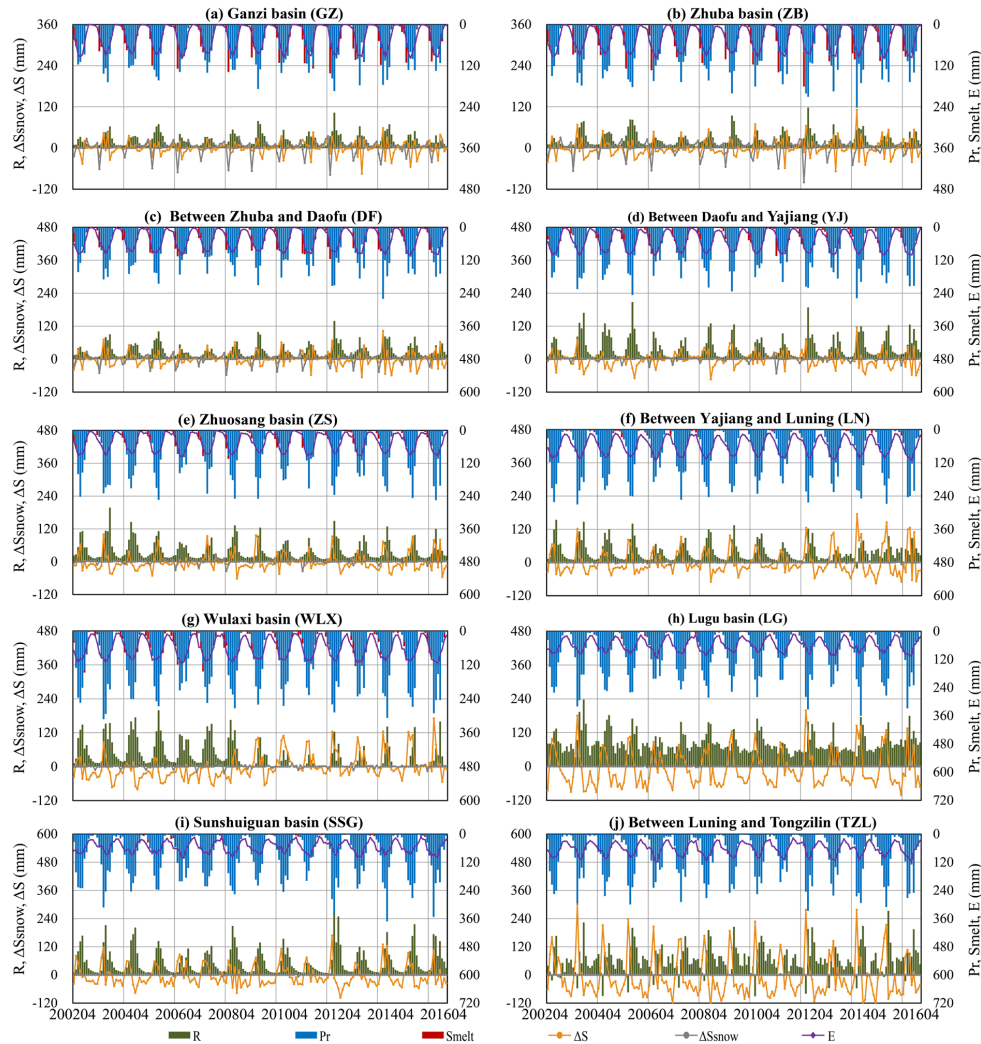


**Figure 3.** Time series of runoff ( $R$ ), rainfall ( $P_r$ ), snowmelt ( $S_{melt}$ ), total storage change ( $\Delta S$ ), snow storage

325 change ( $\Delta S_{snow}$ ) and evapotranspiration ( $E$ ) from 2002 to 2016 in the 10 sub-basins.

To further examine the intra-annual characteristics of key hydrological variables, Figure 4 illustrates the average monthly time series of  $P$ ,  $P_r$ ,  $S_{melt}$ ,  $\Delta S$ ,  $E$ , and  $R$  across the 10 sub-basins from 2002 to 2016. Differences between  $P$  and  $P_r$  are due to  $P_s$  and occurred primarily in the middle and upper regions including GZ and ZB during October to April. The  $S_{melt}$ , which



330 is mainly caused by rising spring temperatures, reflects a delayed impact of  $P_s$  on runoff. Peak values of  $S_{melt}$  occurred between March and May. Constrained by the potential evapotranspiration and water supply conditions,  $E$  steadily increased from January to July, reaching its peak value in July before declining until December.  $R$  was positively correlated to  $P_r$  as shown in Section 3.2, while  $\Delta S$  primarily was positive during spring and summer, 335 reflecting water storage. The contrasting negative  $\Delta S$  during autumn and winter reflects water release. The maximum positive value of  $\Delta S$  was typically observed in June because of the  $P_r$  and  $S_{melt}$  characteristics. The intra-annual variability of  $\Delta S$  was more pronounced in the downstream basin compared to the upstream, which emphasizes the increasing impacts of flow regulation. The net  $R$  in the nested TZL-catchment exhibited a minimum (negative) value in 340 June, coinciding with a maximum value of  $\Delta S$ . This reflects a situation where the local water storage consists of considerable water volumes created upstream of the nested catchment itself. Such storage ensured high  $R$  in LG and TZL during the dry season.

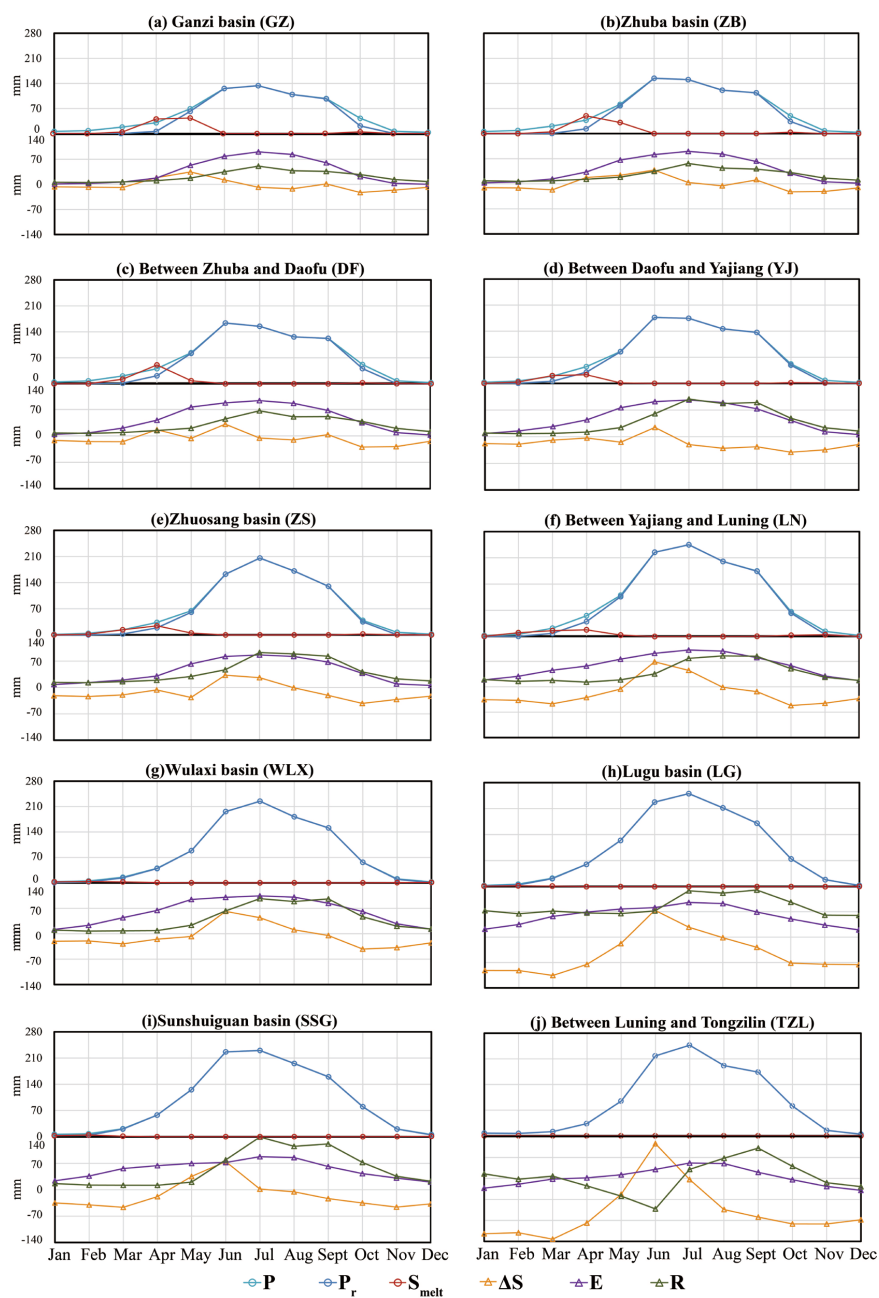


**Figure 4.** Annual average monthly  $P$ ,  $P_r$ ,  $S_{melt}$ ,  $\Delta S$ ,  $E$ , and  $R$  from 2002 to 2016.

345

The relative contribution of the different water balance terms varies across seasons and





regions (Figure S1).  $P_r$  was generally the main contributor across catchments during May-October, while in most catchments  $\Delta S'$  was the main contributor during January-April and November-December. It is noteworthy to mention that the proportions of  $P_r$  and  $S_{melt}$  in the high elevation catchments of GZ (in January, February, November, and December), ZB (in January, February, and December), DF (in January and December), and YJ (in December) were all 0%, as snow accumulation due to temperatures below 0°C essentially prevented effective water input into these basins. During this period,  $\Delta S'$  were primarily driven by the output terms of  $R$  and  $E$ , although their values were low (Fig. 4).

### 3.2. Monthly runoff response to different factors

Partial correlation analysis was conducted after detrending to examine relationships between monthly  $R$  and each of its driving factors  $P_r$ ,  $S_{melt}$ ,  $\Delta S$ , and  $E$ . As shown in Figure 5, the results revealed strong positive correlations between  $R$  and  $P_r$ , however mainly around the summer period (May-Sept) only. There were considerable differences between the catchments, with the highest correlation coefficient observed for the low-elevation small headwater catchment of SSG between March and September (reaching 0.87 in May) and the overall lowest correlations found in the large central and nested catchment of LN where statistical significance was only obtained for May. Conversely, robust negative correlations between  $R$  and  $\Delta S$  were observed from September to January. The correlations were remarkably strong throughout almost all subcatchments. They were e.g. significant in 8 out of 10 catchments in November, 10 out of 10 in December (including a peak correlation of -0.98 in TZL), and 9 out of 10 in January. The effect reflects an increased dominance of  $\Delta S$  as a source of  $R$ , which is in wintertime can be explained by negligible  $P_r$ ,  $S_{melt}$  and  $E$ . Furthermore, in the downstream



catchments including LG and TZL,  $\Delta S$  continues to be a dominating source of  $R$  throughout the year, reflecting that  $\Delta S$  most likely boosted by reservoir storage to values well above those  
370 of  $P_r$ ,  $S_{melt}$  and  $E$ . This is hence in contrast to upstream catchments including GZ, ZB, DF, YJ, and ZS, which with few exceptions do not exhibit significant correlations between  $R$  and  $\Delta S$  between March and August. From January to May,  $S_{melt}$  served as an additional contributor to locally created  $R$  during one or more months in all sub-basins except for the downstream-most TZL (Fig. 5). Regarding correlations between  $R$  and  $E$  they were found to be positive  
375 particularly in spring and early summer, probably because an increased availability of effective water supports simultaneous increases in  $R$  and  $E$ . In August however, correlations were negative in all of the investigated basins (Fig. 5) implying pronounced losses to the atmosphere.

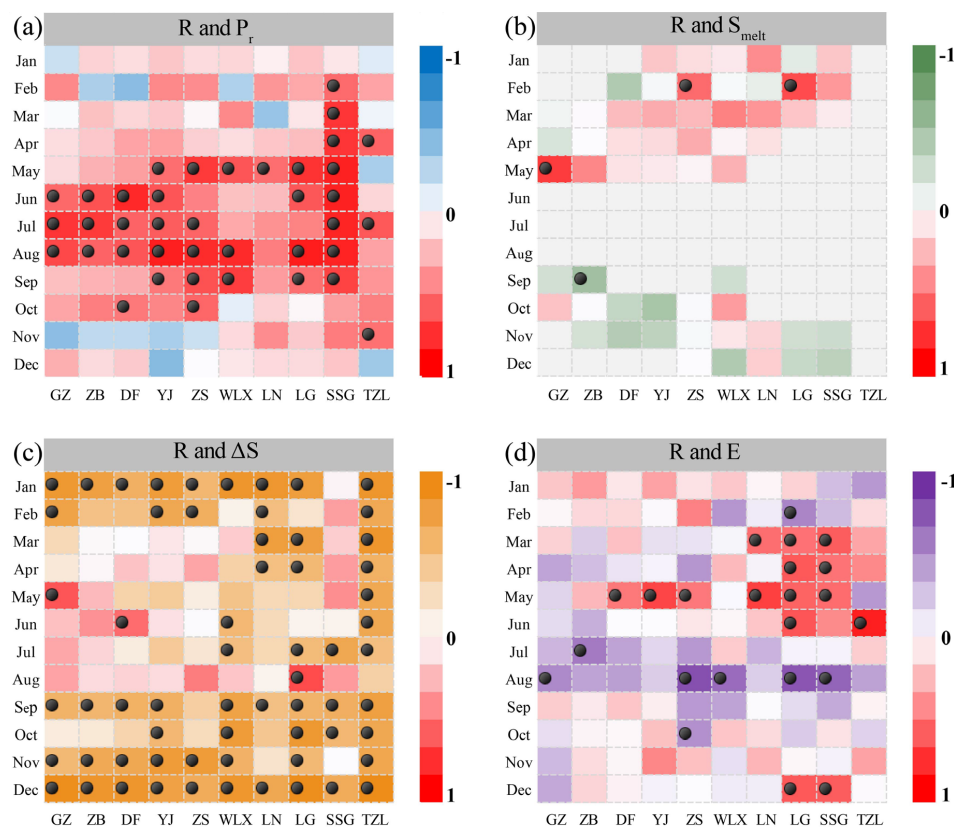


**Figure 5.** Correlation matrices between monthly  $R$  and its driving factors ( $P_r$ ,  $S_{melt}$ ,  $\Delta S$ , and  $E$ ) during the 2002–2016 period in all sub-basins (GZ to TZL). The colors indicate the degree of correlation with darker colors reflecting stronger correlations. The dots represent significant correlations ( $p \leq 0.05$ ).

The delayed effect of  $P$  on  $R$  was investigated considering the entire study period from 2002 to 2016 (Fig. 6). When  $\tau = 0$ , indicating  $R$  responses to  $P$  in the same month, the upper and middle reaches of the basin exhibited higher correlations, with the headwater catchments of GZ (0.85), ZS (0.84), and WLX (0.74) showing significant correlations. Conversely, LN (0.67), LG (0.60), and TZL (0.2) had relatively lower correlation coefficient values. A delay of  $\tau = 1$  resulted in better  $P$ – $R$  correlations for many basins, including all of the nested (non-



headwater) basins DF (0.84), YJ (0.83), LN (0.82), and TZL (0.5) of which the latter two  
 additionally contain hydropower dams. However, as the lag time increased to 2 and 3 months,  
 390 correlations significantly started to weaken, except for the downstream-most TZL, which  
 showed the most significant correlation (0.61) at a lag of two months. These results demonstrate  
 that upstream mountainous headwater catchments on average exhibited relatively prompt  $R$   
 responses to  $P$ , despite seasonal snow storage, whereas ( $\tau \geq 1$ ) in downstream nested  
 catchments including those containing hydropower dams that may have effectively altered the  
 395 natural precipitation-runoff response.

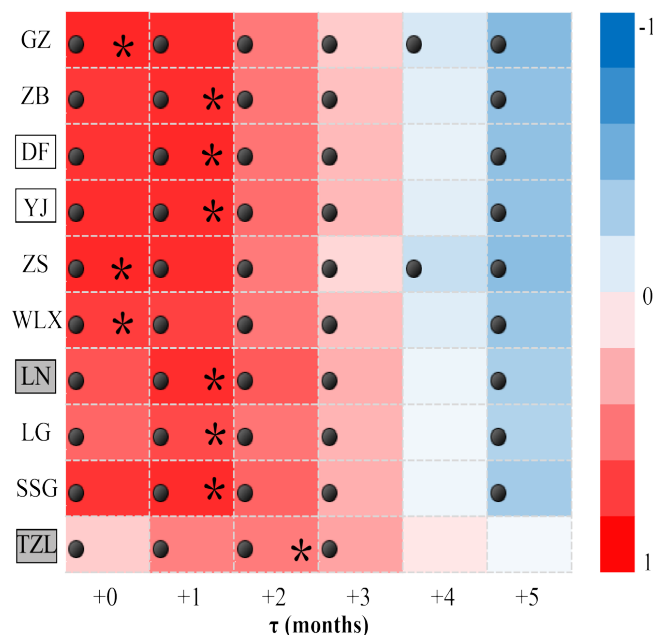


**Figure 6.** Correlation matrix between  $R$  and  $P$  during the period 2002-2016 in all sub-basins (GZ to TZL;  
 nested sub-basins have rectangles around their names, with additional grey shading if they contain  
 hydropower dams). The lagged response in months between  $R$  and  $P$  is denoted “ $\tau$ ”.  $\tau$  degree of correlation  
 400 with darker colors reflecting stronger correlations. The dots represent significant correlations ( $p \leq 0.05$ ). Each



basin's best fitted  $\tau$  is indicated by an asterisk.

### 3.3. Contribution of different factors to runoff variability

Using the Budyko-based variance decomposition method, the influence of various factors on the intra-annual variance of runoff ( $\sigma_R^2$ ) in the ten sub-basins during the period 2002 to 2016 was quantified, as illustrated in Figure 7. The determination coefficients  $R^2$  of all sub-basins were greater than or equal to 0.9, except for LN (0.83), ZS (0.89), and TZL (0.63). The slope of the LG, ZB, and DF were 1.0, while SSG and YJ reached a maximum  $R^2$  of 0.99. Substantially, the variance and covariance of  $P_r$ ,  $S_{melt}$ ,  $E\theta$ , and  $\Delta S'$  effectively captured  $\sigma_R^2$ , which emphasized the significant contribution of these factors to  $\sigma_R^2$ .

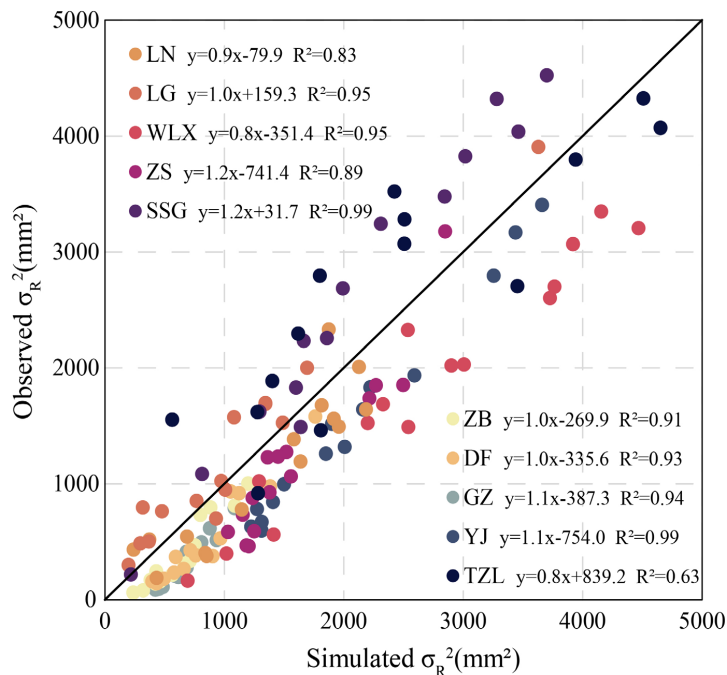


**Figure 7.** Relationships between the observed  $\sigma_R^2$  and the simulated  $\sigma_R^2$  (Eq. 15) using Budyko-based framework in all sub-basins.



Figure 8 illustrates the relative contribution matrix of how variances and covariances of water balance terms contribute to the runoff variance  $\sigma_R^2$ . On average,  $\sigma_{P_r}^2$  was the primary factor driving the intra-annual variance of runoff  $\sigma_R^2$  in the 10 sub-basins, contributing more than 40%, except for TZL (30.2%) and LG (36.6%). The contribution of  $\sigma_{\Delta S'}^2$  to  $\sigma_R^2$  did not exceed 20%, except for TZL (24.3%). Among the covariance contribution of driving factors,  $cov(P_r, \Delta S')$  had a significant impact on  $\sigma_R^2$ , reaching a maximum value of 43.3% in LG. The contributions of other factors were limited, within 10%. These findings indicated that variation in  $P_r$  and  $\Delta S'$  were the primary drivers of intra-annual  $R$  variability in the Yalong River basin, with the contribution of  $P_r$  variation being most prominent in the middle reaches. The impact of  $\Delta S'$  variability was primarily observed downstream, while  $S_{melt}$  variability primarily affected the upstream reaches. The magnitude of contribution of the variances and covariances of the water balance terms to  $R$  variability is presented in Figure S2. The impact of  $\sigma_{E_0}^2$  and  $cov(P_r, S_{melt})$ , on  $\sigma_R^2$  in the upper and middle reaches of the basin was highly volatile. The contribution of  $cov(P_r, \Delta S')$  had a significant negative impact on  $\sigma_R^2$ , reaching a maximum value of -48% in LG, and the contributions of  $cov(P_r, S_{melt})$ ,  $cov(P_r, E_0)$ , and  $cov(S_{melt}, \Delta S')$ , were all in the range of 5 to -20%.



**Figure 8.** Relative contribution matrix of how variances in different water balance terms ( $\sigma_{Pr}^2$ ,  $\sigma_{Smelt}^2$ ,  $\sigma_{E0}^2$ , and  $\sigma_{\Delta S'}^2$ ) and the covariances  $cov(P, S_{melt})$ ,  $cov(P, \Delta S')$ ,  $cov(P, E_0)$ ,  $cov(S_{melt}, \Delta S')$ ,  $cov(S_{melt}, E_0)$ , and  $cov(E_0, \Delta S')$  contribute to runoff variance ( $\sigma_R^2$ ) during the period 2002-2016 in all sub-basins. The colors indicate the degree of contribution.

## 4. Discussion

### 4.1. Contributions of $S_{melt}$ and $\Delta S$ to monthly runoff

This study considered the individual contributions of snow storage  $\Delta S_{snow}$  and other storage components  $\Delta S'$  (reservoirs, lakes, soil water, groundwater) on monthly runoff in the context of the Budyko framework (Bai et al., 2018; Hwang and Devineni, 2022; Shi and Gao, 2022). The findings suggest that  $\Delta S_{snow}$  and the associated meltwater term  $S_{melt}$  played a prominent role as a source of runoff in the spring hydrological processes, which is consistent with other research findings e.g. by Huang et al. (2018). Present results supported previous results also regarding the dominance of  $\Delta S'$  as a source of  $R$  in the downstream regions (Huang

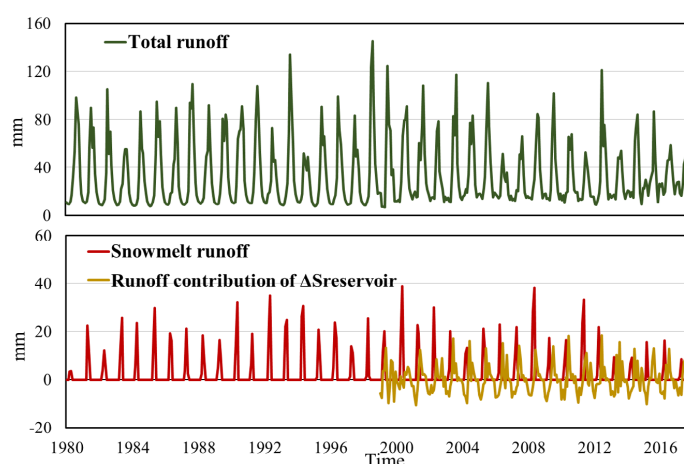


et al., 2021; Xu et al., 2012). This dominance has in recent years has been reinforced by increased storage in hydropower reservoirs within the Yalong River basin (e.g., Huang et al., 2021; Ning et al., 2024; Wu et al., 2024; Xu et al., 2012) However, in contrast to the decreased runoff seasonality that e.g. is found in snow-dominated rivers of central Europe (Rottler et al., 2020), the present study showed that the snow thinning (decreasing  $\Delta S_{snow}$ ; Wu et al., 2024) seen in the upper snow dominated sub-catchments of the Yalong River basin is not yet clearly mirrored in runoff seasonality trends (Figure 3). A contributing factor was found to be the relatively high runoff sensitivity to unfrozen precipitation (rain; Figure 8). Nevertheless, results also showed that, in the upstream Yalong sub-catchments, the seasonal storage of snow still constitutes a large part of the total seasonal water storage (Figure 3). This implies that future runoff seasonality is at risk of decreasing if the climate-driven snow thinning of China's cold regions (Wu et al., 2024; Yang et al., 2015) will continue. Additionally, based on the applied nested catchment/ Budyko approach, this study contributed to disentangling some of the knowledge gaps related to the acknowledged (Fang et al., 2019) complex spatio-temporal runoff patterns in China's cold regions. In particular, we showed that the snow influence propagates to downstream snow-free regions; as e.g. seen in Figure 9, snowmelt contributes approximately 6% to the annual runoff at the Yalong River outlet (Qi et al., 2022). Furthermore, the construction of large reservoirs in 1999 and 2013, mainly in the downstream part of the Yalong River basin, has redistributed the intra-annual runoff pattern of the lower basin (Liu et al., 2019). We here showed that reservoirs contribute approximately 7% to the annual runoff at the Yalong River outlet (Figure 9), primarily during January to April. Hence, snow storage and reservoir storage is currently of about the same importance for monthly runoff characteristics





465 of the entire Yalong River basin, with the relative impact of snow processes and  $S_{melt}$  being considerably larger in its upstream parts. Additionally, since changed snow storage did not yet decrease runoff variability in the snow-covered upstream part of the basin, it cannot have contributed to the recent-year decreases total runoff variability of the entire basin either (Figure 9, top panel).



470

**Figure 9.** Time series of observed total runoff (i.e. monthly discharge volume divided by the total catchment area), runoff contribution of reservoir water storage change (calculated as monthly reservoir storage volume divided by total catchment area) and estimated snowmelt runoff (calculated as the monthly snowmelt volume divided by the total catchment area) from 1980 to 2017 for the whole basin.

475 Regarding water availability present results showed that, for most of the year, there was sufficient water for  $P_r$  to simultaneously replenish both  $R$  and  $\Delta S$ , resulting in a positive correlation between  $P_r$  and  $R$  (Fig. 5a). During the relatively cold dry season,  $R$  was then supplemented by consuming  $\Delta S$  (negative correlation in Fig. 5c), thus highlighting the crucial role of  $\Delta S$  in ensuring the availability of water resources throughout the year (Fig. 4). However,

480 with rising temperatures,  $P_r$  and  $S_{melt}$  will increasingly be partitioned into  $E$  and decreasingly



into  $R$  and/or  $\Delta S$  during prolonged non-frozen (Condon et al., 2020; Zhang et al., 2015). This disturbs the balance of water supply and demand (Zhang et al., 2016) and calls for further research on the availability of  $\Delta S$  to regulate and sufficiently redistribute  $R$  among rainy and dry seasons is essential considering the multiple and partially contrasting needs from energy demand, food demand and other human consumption.

## 4.2. Uncertainties and model performance evaluations

Although the here adopted Choudhury-Yang and Penman-Monteith equations are widely used for actual and potential evapotranspiration, their site-specific applications are associated with uncertainties related to both parameters and processes, such as for instance the understudied evaporation mechanism under snow cover conditions (Gan et al., 2022). Since potential errors in  $E$ -estimations may translate into our  $\Delta S'$ -results when we close water balances, we here independently check the  $E$ -estimation consistency by comparing the simulated  $E$  from the extended Budyko framework with remote sensing-derived  $E$  (GLEAM). The comparison showed good agreement (Table S3), with Nash-Sutcliffe Efficiency (NSE) coefficients exceeding 0.8 for all 10 sub-basins, indicating high model accuracy and reliability. Furthermore, regarding seasonal water supply and demand, the relationship between the monthly ratio of water demand to water supply ( $E/(P_r + S_{melt} - \Delta S')$ ) and monthly ratio of potential water demand to water supply ( $E_0/(P_r + S_{melt} - \Delta S')$ ) as expressed in the extended Budyko framework was further examined for three representative basins: LN, YJ and ZS (Fig S3). Water supply constraints typically occurred in the spring, while water demand constraints were more prevalent in the summer and autumn.

Regarding the partitioning of  $P$  into corresponding  $P_r$  and  $P_s$  components including e.g.



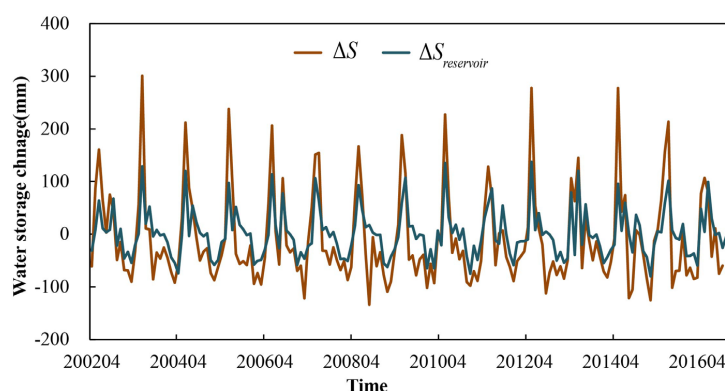
snow melt  $S_{melt}$  processes, we recognize that there are several challenges of determining temperature threshold values. These include impacts of solar radiation on snowmelt (Liu et al., 2017), as well as topography and hydrometeorological factors, particularly in mountainous regions, where topographical elements such as slope, aspect, and mountain cover exert a substantial influence on snow melting (Gan et al., 2022). The energy exchange of snow is furthermore a dynamic process that undergoes temporal variations, leading to discrepancies in the timescales of degree-day factors across different zones (Zhang et al., 2006). In this study, a dataset with the spatial distribution of degree-day factors for glaciers in High Mountain Asia was employed, for which its accuracy had been verified through typical regional simulation applications (Zhang et al., 2016; Zhang et al., 2017). The fact that the degree-day factor method yielded satisfactory simulation results at both daily and monthly time scales (Zhang et al., 2016; 2017) underpins the assumption that our can effectively utilized to calculate monthly snow melt in the here considered Yalong River basin (see also Wu et al., 2024). At the same time, we acknowledge that remaining, difficult-to-reduce process and parameter uncertainties may have non-negligible impacts the presented results.

Facing such remaining uncertainties, we independently ascertained that our main (model-derived) results were consistent with actual, site-specific water storage change outcomes. This was done by collecting and taking advantage of daily storage and release data from several reservoirs within the downstream, nested TZL sub-basin (in which  $\Delta S_{snow}=0$ ). This sub-basin includes the Ertan, Tongzilin and Guandi hydropower reservoirs, which due to their considerable size together represent a large part of the sub-basin's water storage change  $\Delta S$ , making it reasonable to assume that  $\Delta S_{Reservoirs} \approx \Delta S$ . This hence provides a means to constrain



525 and verify our estimates regarding the magnitudes and characteristics of  $\Delta S$  dynamics, which  
were derived through water balance closure. We therefore assessed the agreement between the  
combined monthly storage changes of these reservoirs  $\Delta S_{Reservoirs}$  and our estimated storage  
change  $\Delta S$ , as illustrated in Figure 10. The figure specifically shows that the estimated  
dynamics of  $\Delta S$  fully encloses the amplitudes and reproduces the trends of observed  $\Delta S_{Reservoirs}$ .

530 Regarding the differences in magnitude of storage change, the standard deviation of estimated  
 $\Delta S$  was 86mm, which can be compared with the standard deviation of observed  $\Delta S_{Reservoirs}$  of  
46mm. This hence suggests that reservoirs account for about 53% of the estimated total water  
storage changes, with the missing part originating from unmonitored contributions e.g.  
stemming from storage changes in groundwater reservoirs, unmonitored surface water  
535 reservoirs and soil water. From a methodological viewpoint, we note that the value of 53% also  
provides an upper limit on our possible overestimation of  $\Delta S$ , for the unlikely case that storage  
changes in groundwater reservoirs, unmonitored surface water reservoirs and soil water of TZL  
would in fact be negligible (i.e. approximately equal to 0), such that the differences in storage  
changes between the two curves of Figure 10 would be entirely due to errors in snow melt  
540 modelling and water balance closure. However, even for such lowest possible limit value of  
actual  $\Delta S$ , the storage volumes are still considerable. These findings hence highlight the critical  
role that reservoirs, influenced by human activities, can increasingly play in modulating surface  
water storage in high-mountain areas subject to climate change.



545 **Figure 10.** Time series of estimated storage change ( $\Delta S$ ) and observed reservoir water storage change ( $\Delta S_{Reservoirs}$ ) from 2002 to 2016 within the nested catchment of TZL.

## 5. Conclusions

This study employed an extended Budyko framework in 10 nested catchments of the cold and mountainous Yalong River basin, to analyze spatio-temporal characteristics in water balance terms, and to identify main drivers of monthly runoff variability across an elevation  
 550 gradient (from 5,900 to 1,000 m.a.s.l.). The main findings of this study are:

1) Snow accumulation and snowmelt are main drivers of runoff seasonality in the upper sub-catchments of the Yalong River basin, with propagating impacts also on lower elevation snow-free sub-catchments. These are under increasing additional influence of hydropower  
 555 reservoirs, creating a relatively strong altitudinal heterogeneity in drivers of monthly runoff. This is hypothesized to occur also in other world regions including e.g. major European rivers of Alpine origin, although not yet quantified at similarly high spatio-temporal resolution as in the current study.

2) Presently, snow storage and reservoir storage have approximately equal contributions



560 (6-7% each) to discharge at the Yalong River outlet at its confluence with the Yangtze River,  
implying that both factors need to be accounted for in predictive models.

3) Snow thinning in the high-elevation, snow dominated sub-catchments of the Yalong  
River basin is not yet clearly mirrored in time-series of high-elevation runoff seasonality, e.g.  
due to a considerable runoff sensitivity to unfrozen precipitation.

565 4) The observed lowered runoff seasonality in the lower Yalong River basin (at its  
Yangtze River outlet) is therefore not snow-related and hence likely caused by trends in  
unfrozen precipitation seasonality and/or flow-modulating impacts of constructed reservoirs,  
natural lakes and groundwater, implying that continued snow thinning may further exacerbate  
such trends in the future.

570 5) Regarding lag times, the upstream mountainous headwater catchments of the  
Yalong basin showed relatively prompt R responses to P (less than a month on average) despite  
seasonal snow storage, whereas delays were more significant (i.e., more than a month) in  
downstream nested catchments including those containing man-made reservoirs.

6) Methodologically, we showed by independent verification with reservoir storage data  
575 that the extended monthly Budyko framework could be used to distinguish between water  
storage and seasonal snow accumulation, which has important implications for understanding  
dominant runoff processes, and more generally for mitigating adverse effect related to the rapid  
environmental changes that the Yalong River basin and other cold regions (not least of the  
Tibetan plateau) are currently experiencing.

## 580 **Author Contributions**

N.W. and J.J. conceived the idea and designed the research framework. Z.N. carried out



data collection, preprocessing, and method determination. N.W. and H.H. performed data  
 analysis, graphical visualization, and manuscript preparation. K.Z. and A.N. contributed to  
 manuscript refinement. All authors have read and agreed to the published version of the  
 585 manuscript.

## Acknowledgments

This study was supported by the Fundamental Research Funds for the Central Universities  
 of China: B240203007 and Fund of National Key Laboratory of Water Disaster Prevention:  
 524015222.

## 590 Declaration of competing interest

The authors declare that they have no known competing financial interests or personal  
 relationships that could have appeared to influence the work reported in this paper.

## References

- Allen, R.G., Pereira, L.S., Raes, D., Smith, M., 1998. Crop evapotranspiration-Guidelines for  
 595 computing crop water requirements-FAO Irrigation and drainage paper 56. Food and  
 Agriculture Organization of the United Nations, Rome.
- Bai, J., Li, J., Shi, H., Liu, T., Zhong, R., 2018. Snowmelt Water Alters the Regime of Runoff  
 in the Arid Region of Northwest China. *Water* 10, 902.  
<https://doi.org/10.3390/w10070902>
- 600 Bao, Z., Zhang, Jianyun, Lian, Y., Wang, G., Jin, J., Ning, Z., Zhang, Jiapeng, Liu, Y., Wang,  
 X., 2023. Changes in Headwater Streamflow from Impacts of Climate Change in the  
 Tibetan Plateau. *Engineering*. <https://doi.org/10.1016/j.eng.2023.05.025>
- Berghuijs, W.R., Sivapalan, M., Woods, R.A., Savenije, H.H.G., 2014. Patterns of similarity of  
 seasonal water balances: A window into streamflow variability over a range of time scales.  
 605 *Water Resour. Res.* 50, 5638–5661. <https://doi.org/10.1002/2014WR015692>
- Bounoua, L., DeFries, R.S., Imhoff, M.L., Steininger, M.K., 2004. Land use and local climate:  
 A case study near Santa Cruz, Bolivia. *Meteorol. Atmos. Phys.* 86, 73–85.  
<https://doi.org/10.1007/s00703-003-0616-8>
- Brutsaert, W., Hiyama, T., 2012. The determination of permafrost thawing trends from long-



- term streamflow measurements with an application in eastern Siberia. *J. Geophys. Res.-Atmos.* 117, D22110. <https://doi.org/10.1029/2012JD018344>
- Chao, B.F., Wu, Y.H., Li, Y.S., 2008. Impact of Artificial Reservoir Water Impoundment on Global Sea Level. *Science* 320, 212–214. <https://doi.org/10.1126/science.1154580>
- Chen, D.L., Gao, G., Xu, C.Y., Guo, J., Ren, G.Y., 2005. Comparison of the Thornthwaite method and pan data with the standard Penman-Monteith estimates of reference evapotranspiration in China. *Clim. Res.* 28, 123–132. <https://doi.org/10.3354/cr028123>
- Choudhury, B.J., 1999. Evaluation of an empirical equation for annual evaporation using field observations and results from a biophysical model. *J. Hydrol.* 216, 99–110. [https://doi.org/10.1016/S0022-1694\(98\)00293-5](https://doi.org/10.1016/S0022-1694(98)00293-5)
- Condon, L.E., Atchley, A.L., Maxwell, R.M., 2020. Evapotranspiration depletes groundwater under warming over the contiguous United States. *Nat. Commun.* 11, 873. <https://doi.org/10.1038/s41467-020-14688-0>
- Cui, T., Li, Y., Yang, L., Nan, Y., Li, K., Tudaji, M., Hu, H., Long, D., Shahid, M., Mubeen, A., He, Z., Yong, B., Lu, H., Li, C., Ni, G., Hu, C., Tian, F., 2023. Non-monotonic changes in Asian Water Towers' streamflow at increasing warming levels. *Nat. Commun.* 14, 1176. <https://doi.org/10.1038/s41467-023-36804-6>
- Dethier, E.N., Sartain, S.L., Renshaw, C.E., Magilligan, F.J., 2020. Spatially coherent regional changes in seasonal extreme streamflow events in the United States and Canada since 1950. *Sci. Adv.* 6, eaba5939. <https://doi.org/10.1126/sciadv.aba5939>
- Du, C., Sun, F., Yu, J., Liu, X., Chen, Y., 2016. New interpretation of the role of water balance in an extended Budyko hypothesis in arid regions. *Hydrol. Earth Syst. Sci.* 20, 393–409. <https://doi.org/10.5194/hess-20-393-2016>
- Fang, H., Huang, L., Wang, J., He, G., Reible, D., 2016. Environmental assessment of heavy metal transport and transformation in the Hangzhou Bay, China. *J. Hazard. Mater.* 302, 447–457. <https://doi.org/10.1016/j.jhazmat.2015.09.060>
- Fang, Y., Li, H., Wan, W., Zhu, S., Wang, Z., Hong, Y., Wang, H., 2019. Assessment of Water Storage Change in China's Lakes and Reservoirs over the Last Three Decades. *Remote Sens.* 11, 1467. <https://doi.org/10.3390/rs11121467>
- Gan, G., Wu, J., Hori, M., Fan, X., Liu, Y., 2022. Attribution of decadal runoff changes by considering remotely sensed snow/ice melt and actual evapotranspiration in two contrasting watersheds in the Tianshan Mountains. *J. Hydrol.* 610, 127810. <https://doi.org/10.1016/j.jhydrol.2022.127810>
- Gao, H., Ding, Y., Zhao, Q., Hrachowitz, M., Savenije, H.H.G., 2017. The importance of aspect for modelling the hydrological response in a glacier catchment in Central Asia. *Hydrol. Process.* 31, 2842–2859. <https://doi.org/10.1002/hyp.11224>
- Guo, W., Teng, Y., Li, J., Yan, Y., Zhao, C., Li, Y., Li, X., 2024. A new assessment framework to forecast land use and carbon storage under different SSP-RCP scenarios in China. *Science of The Total Environment* 912, 169088. <https://doi.org/10.1016/j.scitotenv.2023.169088>
- Gutenson, J.L., Tavakoly, A.A., Wahl, M.D., Follum, M.L., 2020. Comparison of generalized non-data-driven lake and reservoir routing models for global-scale hydrologic forecasting of reservoir outflow at diurnal time steps. *Hydrol. Earth Syst. Sci.* 24, 2711–2729.





- <https://doi.org/10.5194/hess-24-2711-2020>
- 655 Han, P., Long, D., Han, Z., Du, M., Dai, L., Hao, X., 2019. Improved understanding of snowmelt runoff from the headwaters of China's Yangtze River using remotely sensed snow products and hydrological modeling. *Remote Sens. Environ.* 224, 44–59. <https://doi.org/10.1016/j.rse.2019.01.041>
- 660 He, Z., Zhang, X., Bao, S., Qiao, Y., Sheng, Y., Liu, X., He, X., Yang, X., Zhao, J., Liu, R., Lu, C., 2015. Multiple climatic cycles imprinted on regional uplift-controlled fluvial terraces in the lower Yalong River and Anning River, SE Tibetan Plateau. *Geomorphology* 250, 95–112. <https://doi.org/10.1016/j.geomorph.2015.08.010>
- Hock, R., 2003. Temperature index melt modelling in mountain areas. *J. Hydrol.* 282, 104–115. [https://doi.org/10.1016/S0022-1694\(03\)00257-9](https://doi.org/10.1016/S0022-1694(03)00257-9)
- 665 Huang, P., Song, J., Cheng, D., Sun, H., Kong, F., Jing, K., Wu, Q., 2021. Understanding the intra-annual variability of streamflow by incorporating terrestrial water storage from GRACE into the Budyko framework in the Qinba Mountains. *J. Hydrol.* 603, 126988. <https://doi.org/10.1016/j.jhydrol.2021.126988>
- Huang, Y., Zhao, H., Jiang, Y., Lu, X., 2018. Runoff and its influencing factors in the upper reaches of the Yalong River. *Arid Land Geo.* 41, 127–133. <https://doi.org/10.13826/j.cnki.cn65-1103/x.2018.01.016>
- 670 Huo, J., Liu, C., Yu, X., Jia, G., Chen, L., 2021. Effects of watershed char and climate variables on annual runoff in different climatic zones in China. *Sci. Total Environ.* 754, 142157. <https://doi.org/10.1016/j.scitotenv.2020.142157>
- 675 Hwang, J., Devineni, N., 2022. An Improved Zhang's Dynamic Water Balance Model Using Budyko-Based Snow Representation for Better Streamflow Predictions. *Water Resour. Res.* 58, e2021WR030203. <https://doi.org/10.1029/2021WR030203>
- Kazemi, H., Hashemi, H., Maghsood, F.F., Hosseini, S.H., Sarukkalige, R., Jamali, S., Berndtsson, R., 2021. Climate vs. Human Impact: Quantitative and Qualitative Assessment of Streamflow Variation. *Water* 13, 2404. <https://doi.org/10.3390/w13172404>
- 680 Kuhn, M., Helfricht, K., Ortner, M., Landmann, J., Gurgiser, W., 2016. Liquid water storage in snow and ice in 86 Eastern Alpine basins and its changes from 1970-97 to 1998-2006. *Ann. Glaciol.* 57, 11–18. <https://doi.org/10.1017/aog.2016.24>
- 685 Li, L., Ni, J., Chang, F., Yue, Y., Frolova, N., Magritsky, D., Borthwick, A.G.L., Ciais, P., Wang, Y., Zheng, C., Walling, D.E., 2020. Global trends in water and sediment fluxes of the world's large rivers. *Sci. Bull.* 65, 62–69. <https://doi.org/10.1016/j.scib.2019.09.012>
- Li, X., Zhang, K., Gu, P., Feng, H., Yin, Y., Chen, W., Cheng, B., 2021. Changes in precipitation extremes in the Yangtze River Basin during 1960-2019 and the association with global warming, ENSO, and local effects. *Sci. Total Environ.* 760, 144244. <https://doi.org/10.1016/j.scitotenv.2020.144244>
- 690 Li, Z., Quiring, S.M., 2021. Investigating spatial heterogeneity of the controls of surface water balance in the contiguous United States by considering anthropogenic factors. *J. Hydrol.* 601, 126621. <https://doi.org/10.1016/j.jhydrol.2021.126621>
- 695 Liu, J., You, Y., Zhang, Q., Gu, X., 2021. Attribution of streamflow changes across the globe based on the Budyko framework. *Sci. Total Environ.* 794, 148662. <https://doi.org/10.1016/j.scitotenv.2021.148662>



- Liu, J., Zhang, Q., Feng, S., Gu, X., Singh, V.P., Sun, P., 2019. Global Attribution of Runoff Variance Across Multiple Timescales. *J. Geophys. Res.-Atmos.* 124, 13962–13974. <https://doi.org/10.1029/2019JD030539>
- 700 Liu, J., Zhang, Q., Singh, V.P., Shi, P., 2017. Contribution of multiple climatic variables and human activities to streamflow changes across China. *J. Hydrol.* 545, 145–162. <https://doi.org/10.1016/j.jhydrol.2016.12.016>
- Liu, J., Zhang, Q., Singh, V.P., Song, C., Zhang, Y., Sun, P., Gu, X., 2018. Hydrological effects of climate variability and vegetation dynamics on annual fluvial water balance in global large river basins. *Hydrol. Earth Syst. Sci.* 22, 4047–4060. [https://doi.org/10.5194/hess-](https://doi.org/10.5194/hess-22-4047-2018)  
 705 22-4047-2018
- Liu, X., Yang, M., Meng, X., Wen, F., Sun, G., 2019. Assessing the Impact of Reservoir Parameters on Runoff in the Yalong River Basin using the SWAT Model. *Water* 11, 643. <https://doi.org/10.3390/w11040643>
- 710 Liu, Z., Wang, T., Han, J., Yang, W., Yang, H., 2022. Decreases in Mean Annual Streamflow and Interannual Streamflow Variability Across Snow-Affected Catchments Under a Warming Climate. *Geophys. Res. Lett.* 49, e2021GL097442. <https://doi.org/10.1029/2021GL097442>
- Luo, M., Lau, N.-C., 2018. Synoptic characteristics, atmospheric controls, and long-term changes of heat waves over the Indochina Peninsula. *Clim. Dyn.* 51, 2707–2723. <https://doi.org/10.1007/s00382-017-4038-6>  
 715 <https://doi.org/10.1007/s00382-017-4038-6>
- Lute, A.C., Abatzoglou, J.T., 2014. Role of extreme snowfall events in interannual variability of snowfall accumulation in the western United States. *Water Resour. Res.* 50, 2874–2888. <https://doi.org/10.1002/2013WR014465>
- 720 Miralles, D.G., De Jeu, R. a. M., Gash, J.H., Holmes, T.R.H., Dolman, A.J., 2011. Magnitude and variability of land evaporation and its components at the global scale. *Hydrol. Earth Syst. Sci.* 15, 967–981. <https://doi.org/10.5194/hess-15-967-2011>
- New, M., Hulme, M., Jones, P., 2000. Representing twentieth-century space-time climate variability. Part II: Development of 1901–96 monthly grids of terrestrial surface climate. *J. Clim.* 13, 2217–2238. [https://doi.org/10.1175/1520-](https://doi.org/10.1175/1520-0442(2000)013<2217:RTCSTC>2.0.CO;2)  
 725 0442(2000)013<2217:RTCSTC>2.0.CO;2
- Ning, T., Li, Z., Liu, W., 2017. Vegetation dynamics and climate seasonality jointly control the interannual catchment water balance in the Loess Plateau under the Budyko framework. *Hydrol. Earth Syst. Sci.* 21, 1515–1526. <https://doi.org/10.5194/hess-21-1515-2017>
- 730 Ning, Z., Wu, N., Zhang, J., Ruan, Y., Tang, Z., Sun, J., Shi, J., Liu, C., Wang, G., 2024. Wetter trend in source region of Yangtze River by runoff simulating based on Grid-RCCC-WBM. *J. Hydrol.* 631, 130702. <https://doi.org/10.1016/j.jhydrol.2024.130702>
- Qi, W., Feng, L., Kuang, X., Zheng, C., Liu, J., Chen, D., Tian, Y., Yao, Y., 2022. Divergent and Changing Importance of Glaciers and Snow as Natural Water Reservoirs in the Eastern and Southern Tibetan Plateau. *J. Geophys. Res.-Atmos.* 127, e2021JD035888. <https://doi.org/10.1029/2021JD035888>  
 735 <https://doi.org/10.1029/2021JD035888>
- Rottler, E., Francke, T., Buerger, G., Bronstert, A., 2020. Long-term changes in central European river discharge for 1869–2016: impact of changing snow covers, reservoir constructions and an intensified hydrological cycle. *Hydrol. Earth Syst. Sci.* 24, 1721–



1740. <https://doi.org/10.5194/hess-24-1721-2020>
- 740 Shen, C., 2018. A Transdisciplinary Review of Deep Learning Research and Its Relevance for  
 Water Resources Scientists. *Water Resour. Res.* 54, 8558–8593.  
<https://doi.org/10.1029/2018WR022643>
- Shi, G., Gao, B., 2022. Attribution Analysis of Runoff Change in the Upper Reaches of the  
 Kaidu River Basin Based on a Modified Budyko Framework. *Atmosphere* 13, 1385.  
 745 <https://doi.org/10.3390/atmos13091385>
- Stigter, E.E., Litt, M., Steiner, J.F., Bonekamp, P.N.J., Shea, J.M., Bierkens, M.F.P., Immerzeel,  
 W.W., 2018. The Importance of Snow Sublimation on a Himalayan Glacier. *Front. Earth  
 Sci.* 6, 108. <https://doi.org/10.3389/feart.2018.00108>
- Tu, X., Singh, V.P., Chen, X., Chen, L., Zhang, Q., Zhao, Y., 2015. Intra-annual Distribution of  
 750 Streamflow and Individual Impacts of Climate Change and Human Activities in the  
 Dongjiang River Basin, China. *Water Resour. Manag.* 29, 2677–2695.  
<https://doi.org/10.1007/s11269-015-0963-5>
- Wang, D., Tang, Y., 2014. A one-parameter Budyko model for water balance captures emergent  
 behavior in darwinian hydrologic models. *Geophys. Res. Lett.* 41, 4569–4577.  
 755 <https://doi.org/10.1002/2014GL060509>
- Wang, Z., Wu, R., Chen, S., Huang, G., Liu, G., Zhu, L., 2018. Influence of Western Tibetan  
 Plateau Summer Snow Cover on East Asian Summer Rainfall. *J. Geophys. Res.-Atmos.*  
 123, 2371–2386. <https://doi.org/10.1002/2017JD028016>
- Widen-Nilsson, E., Halldin, S., Xu, C., 2007. Global water-balance modelling with WASMOD-  
 760 M: Parameter estimation and regionalisation. *J. Hydrol.* 340, 105–118.  
<https://doi.org/10.1016/j.jhydrol.2007.04.002>
- Wu, C., Yeh, P.J.-F., Hu, B.X., Huang, G., 2018. Controlling factors of errors in the predicted  
 annual and monthly evaporation from the Budyko framework. *Adv. Water Resour.* 121,  
 432–445. <https://doi.org/10.1016/j.advwatres.2018.09.013>
- 765 Wu, C., Yeh, P.J.-F., Wu, H., Hu, B.X., Huang, G., 2019. Global Analysis of the Role of  
 Terrestrial Water Storage in the Evapotranspiration Estimated from the Budyko  
 Framework at Annual to Monthly Time Scales. *J. Hydrometeorol.* 20, 2003–2021.  
<https://doi.org/10.1175/JHM-D-19-0065.1>
- Wu, N., Zhang, K., Chao, L., Ning, Z., Wang, S., Jarsjö, J., 2024. Snow cover expansion with  
 770 contrasting depth thinning in the recent 40 years: Evidence from the Yalong River Basin,  
 South-eastern Tibetan Plateau. *J. Hydrol.-Reg. Stud.* 53, 101786.  
<https://doi.org/10.1016/j.ejrh.2024.101786>
- Wu S., Shen M., 2007. The key technical issue and its research advance in Yalong River  
 hydropower development. *J. Hydraul. Eng.* 15–19.
- 775 Wu, Z., Li, J., Jiang, Z., Ma, T., 2012. Modulation of the Tibetan Plateau Snow Cover on the  
 ENSO Teleconnections: From the East Asian Summer Monsoon Perspective. *J. Clim.* 25,  
 2481–2489. <https://doi.org/10.1175/JCLI-D-11-00135.1>
- Wulf, H., Bookhagen, B., Scherler, D., 2016. Differentiating between rain, snow, and glacier  
 contributions to river discharge in the western Himalaya using remote-sensing data and  
 780 distributed hydrological modeling. *Adv. Water Resour.* 88, 152–169.  
<https://doi.org/10.1016/j.advwatres.2015.12.004>



- Xin, J., Sun, X., Liu, L., Li, H., Liu, X., Li, X., Cheng, L., Xu, Z., 2021. Quantifying the contribution of climate and underlying surface changes to alpine runoff alterations associated with glacier melting. *Hydrol. Process.* 35, e14069. <https://doi.org/10.1002/hyp.14069>
- 785 Xin, Z., Li, Y., Zhang, L., Ding, W., Ye, L., Wu, J., Zhang, C., 2019. Quantifying the relative contribution of climate and human impacts on seasonal streamflow. *J. Hydrol.* 574, 936–945. <https://doi.org/10.1016/j.jhydrol.2019.04.095>
- Xu, X., Yang, D., Sivapalan, M., 2012. Assessing the impact of climate variability on catchment water balance and vegetation cover. *Hydrol. Earth Syst. Sci.* 16, 43–58. <https://doi.org/10.5194/hess-16-43-2012>
- 790 Xu, X., Yang, D., Yang, H., Lei, H., 2014. Attribution analysis based on the Budyko hypothesis for detecting the dominant cause of runoff decline in Haihe basin. *J. Hydrol.* 510, 530–540. <https://doi.org/10.1016/j.jhydrol.2013.12.052>
- 795 Yang, H., Yang, D., Lei, Z., Sun, F., 2008. New analytical derivation of the mean annual water-energy balance equation. *Water Resour. Res.* 44, W03410. <https://doi.org/10.1029/2007WR006135>
- Yang, T., Wang, C., Chen, Y., Chen, X., Yu, Z., 2015. Climate change and water storage variability over an arid endorheic region. *J. Hydrol.* 529, 330–339. <https://doi.org/10.1016/j.jhydrol.2015.07.051>
- 800 Yang, Z., Bai, P., 2023. Evaporation from snow surface: A multi-model evaluation with the FLUXNET2015 dataset. *J. Hydrol.* 621, 129587. <https://doi.org/10.1016/j.jhydrol.2023.129587>
- Yao, L., Libera, D.A., Kheimi, M., Sankarasubramanian, A., Wang, D., 2020. The Roles of Climate Forcing and Its Variability on Streamflow at Daily, Monthly, Annual, and Long-Term Scales. *Water Resour. Res.* 56. <https://doi.org/10.1029/2020WR027111>
- 805 Ye, S., Li, H.-Y., Li, S., Leung, L.R., Demissie, Y., Ran, Q., Bloeschl, G., 2015. Vegetation regulation on streamflow intra-annual variability through adaption to climate variations. *Geophys. Res. Lett.* 42, 10307–10315. <https://doi.org/10.1002/2015GL066396>
- 810 Zeng, R., Cai, X., 2015. Assessing the temporal variance of evapotranspiration considering climate and catchment storage factors. *Adv. Water Resour.* 79, 51–60. <https://doi.org/10.1016/j.advwatres.2015.02.008>
- Zhang, D., Cong, Z., Ni, G., Yang, D., Hu, S., 2015. Effects of snow ratio on annual runoff within the Budyko framework. *Hydrol. Earth Syst. Sci.* 19, 1977–1992. <https://doi.org/10.5194/hess-19-1977-2015>
- 815 Zhang, D., Liu, X., Zhang, Q., Liang, K., Liu, C., 2016. Investigation of factors affecting intra-annual variability of evapotranspiration and streamflow under different climate conditions. *J. Hydrol.* 543, 759–769. <https://doi.org/10.1016/j.jhydrol.2016.10.047>
- Zhang, K., Kimball, J.S., Nemani, R.R., Running, S.W., Hong, Y., Gourley, J.J., Yu, Z., 2015. Vegetation Greening and Climate Change Promote Multidecadal Rises of Global Land Evapotranspiration. *Sci Rep* 5, 15956. <https://doi.org/10.1038/srep15956>
- 820 Zhang, L., Hickel, K., Dawes, W.R., Chiew, F.H.S., Western, A.W., Briggs, P.R., 2004. A rational function approach for estimating mean annual evapotranspiration. *Water Resour. Res.* 40, W02502. <https://doi.org/10.1029/2003WR002710>



- 825 Zhang, L., Potter, N.J., Zhang, Y., 2010. Water balance modeling over variable time scales  
 based on the Budyko framework - Model development and testing (vol 360, pg 117, 2008).  
 J. Hydrol. 390, 121–122. <https://doi.org/10.1016/j.jhydrol.2010.05.027>
- Zhang, L., Su, F., Yang, D., Hao, Z., Tong, K., 2013. Discharge regime and simulation for the  
 upstream of major rivers over Tibetan Plateau. J. Geophys. Res.-Atmos. 118, 8500–8518.  
 830 <https://doi.org/10.1002/jgrd.50665>
- Zhang, S., Yang, H., Yang, D., Jayawardena, A.W., 2016. Quantifying the effect of vegetation  
 change on the regional water balance within the Budyko framework. Geophysical  
 Research Letters 43, 1140–1148. <https://doi.org/10.1002/2015GL066952>
- Zhang, X., Dong, Q., Zhang, Q., Yu, Y., 2020. A unified framework of water balance models  
 835 for monthly, annual, and mean annual timescales. J. Hydrol. 589, 125186.  
<https://doi.org/10.1016/j.jhydrol.2020.125186>
- Zhang, Y., Enomoto, H., Ohata, T., Kitabata, H., Kadota, T., Hirabayashi, Y., 2017. Glacier  
 mass balance and its potential impacts in the Altai Mountains over the period 1990–2011.  
 J. Hydrol. 553, 662–677. <https://doi.org/10.1016/j.jhydrol.2017.08.026>
- 840 Zhang, Y., Liu, S., Ding, Y., 2006. Spatial variation of degree-day factors on the observed  
 glaciers in western China. Acta Geographica Sinica 61, 89.
- Zhang, Y., Liu, S., Wang, X., 2019. A dataset of spatial distribution of degree-day factors for  
 glaciers in High Mountain Asia. China Sci. Data 4, 141–151.  
<https://doi.org/10.11922/csdata.2019.0009.zh>

845